Infrared Multi-Object Spectrograph of MOIRCS

Chihiro Tokoku[ab], Ryuji Suzuki[ab], Koji Omata[a], Masahiro Konishi[ab], Tomohiro Yoshikawa[ab], Masayuki Akiyama[a], Ichi Tanaka[ab], Takashi Ichikawa[b], and Tetsuo Nishimura[a]

[a]Subaru Telescope, 650 N. Aohoku Pl., Hilo, HI 96720, U.S.A.;
[b]Astronomical Institute, Tohoku University, Aramaki, Aoba-ku, Sendai 980-8578, Japan

ABSTRACT

The design, development, operation and current performance of MOS (multi-object spectroscopy) mode of MOIRCS is described. MOIRCS (Multi-Object Infrared Camera and Spectrograph) is one of the second-generation instruments for the Subaru Telescope and provides imaging and MOS modes with a $4' \times 7'$ field of view for a wavelength range from 0.85 to 2.5 μm. To achieve near-infrared(NIR) MOS up to K-band, MOS mode uses multi-slit masks and a mask exchange system in a cryogenic environment. The masks are housed in a vacuum dewar attached to the MOIRCS main dewar and separated by a large gate valve. The mask dewar is equipped with its own cryogenic cooler and a vacuum pump and is capable of storing eighteen masks. The masks are made of thin aluminum foil. Slits are cut with a laser, with software that corrects for the effects of thermal contraction. The masks are cooled to below 130 K in the mask dewar and transported to the focal plane in the main dewar through the gate valve with a linear motion manipulator. An interlock is equipped on the mask exchange system to secure the cryogenic instrument from accident. Replacing masks can be done in the daytime without breaking the vacuum of the main dewar by isolating the mask dewar with the gate valve. Acquisition occurs by iteratively taking on-sky images through alignment holes on the mask until the rotation and offset between alignment stars and alignment holes become small enough. MOIRCS/MOS mode will be open to the public in late 2006.

Keywords: near infrared, multi-object spectroscopy, multi-slit mask

1. INTRODUCTION

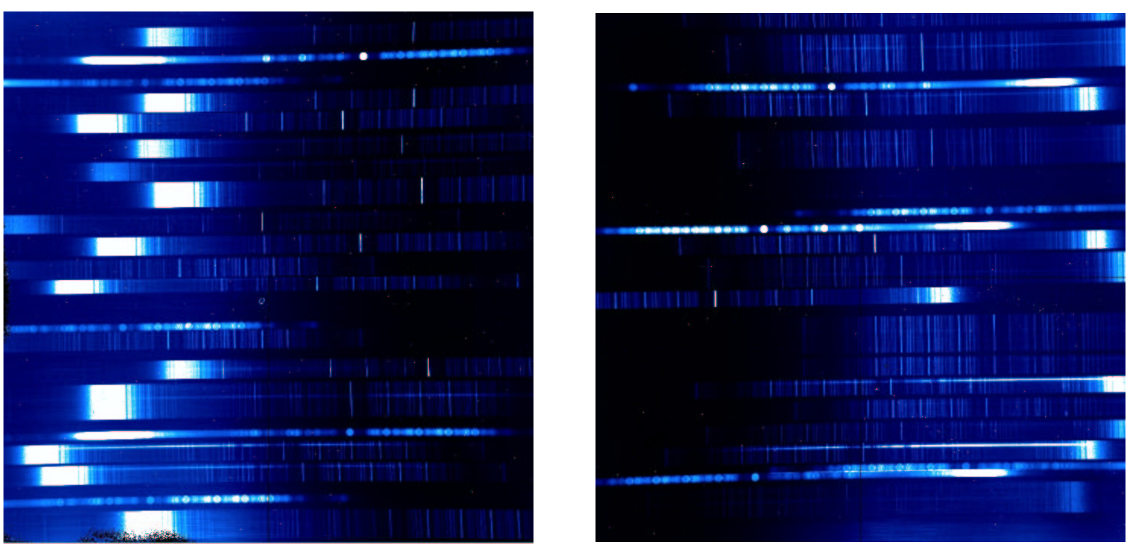

Figure 1. An example of a multi-slit image taken with MOIRCS during test observations in December, 2005. More than 30 objects on one mask have been observed simultaneously with a spectral resolution $R{\sim}500$.

Correspondence(C.T.): tokoku@subaru.naoj.org

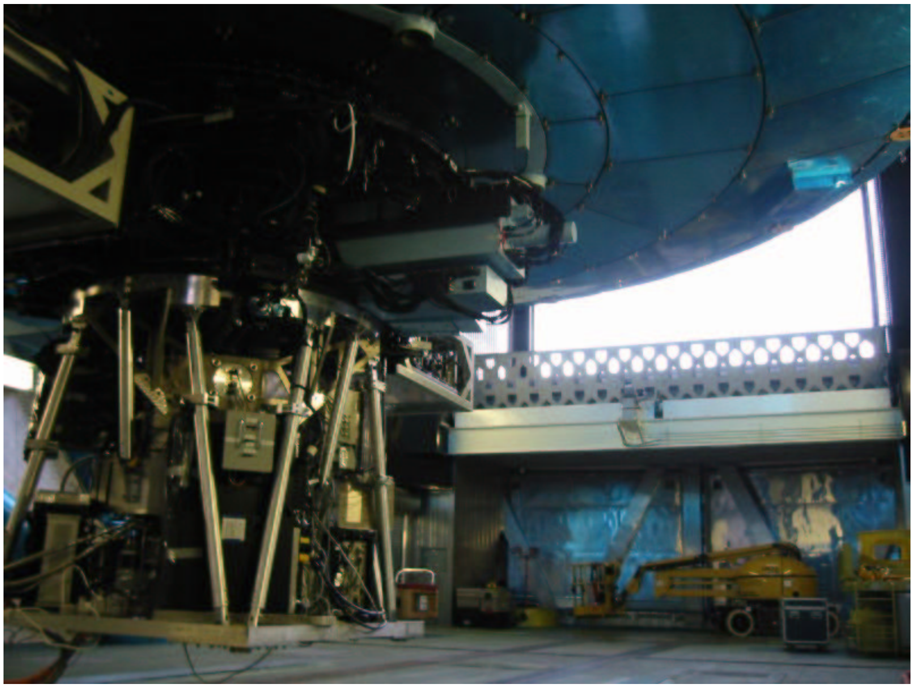

Figure 2. MOIRCS mounted on the Subaru Telescope.

In order to realize a NIR MOS instrument, it is required to overcome several difficulties. First, in order to reduce the thermal background from MOS masks, the masks need to be as cold as 150K. The masks must be cooled uniformly to avoid mask distortion. Therefore, the mask material should have good thermal conductivity. Metals have good thermal conductivity, but it is difficult to make small slits with the necessary $\sim$100 μm widths with sufficient precision. Thus, making the MOS mask itself is difficult. In addition, the mask exchange mechanism for such an instrument needs to work under a cryogenic environment. Under low-temperature and low-pressure, reliable movement is quite restricted. Thus the mask exchange mechanism is another difficulty in a cryogenic MOS instrument. Second, in order to replace MOS masks, a thermal cycle of the cryostat is required. The exchange procedure needs to be done in a reasonable time scale, e.g. a few days at most. But, a typical thermal cycle of a cryogenic instrument takes about a few weeks. We designed the cryogenic MOS system with unique solutions to address the above difficulties.

MOIRCS has imaging capabilities in the wavelength range from 0.85 μm to 2.5 μm with a $4' \times 7'$ field of view (FOV). The focal plane at the Cassegrain focus of the Subaru Telescope is imaged onto two 2048 $\times$ 2048 pixel HAWAII-2 HgCdTe arrays (Rockwell Scientific) with a pixel scale of $0.''117$ pixel^{-1}. The details of the detectors are given in Ichikawa et al.(2003)[1] and Katsuno et al.(2003).[2] The optical design is optimized to maximize the performance in the K-band. All the components of MOIRCS inside the cryostat are cooled to under 100 K. The optical system is designed to work at these temperature with consideration given to the refractive index change of the lens materials at 77 K as small as thermal contraction of the lenses. The details of the optical design are given in Suzuki et al.(2003).[3]

The imaging mode achieved its first light in September 2004 and we confirmed the limiting magnitude of MOIRCS $J\sim$ 23.8 mag, $H\sim$ 22.7 mag, and $Ks \sim$ 21.8 mag for total exposure times of 3600 s with S/N=5 and a $1''$ aperture. Total throughputs of the imaging mode were measured to be $\sim$32% in the H and K-band and $\sim$22% in the J-band including the telescope. The current status and performance of MOIRCS are reported in Ichikawa et al.(2006)[4] in this volume.

MOIRCS has several pairs of grisms for spectroscopic observations; the "zJ500" grism optimized for the z and J-band, while the "HK500" grism optimized for the H and K-bands observations. Both of these grisms are

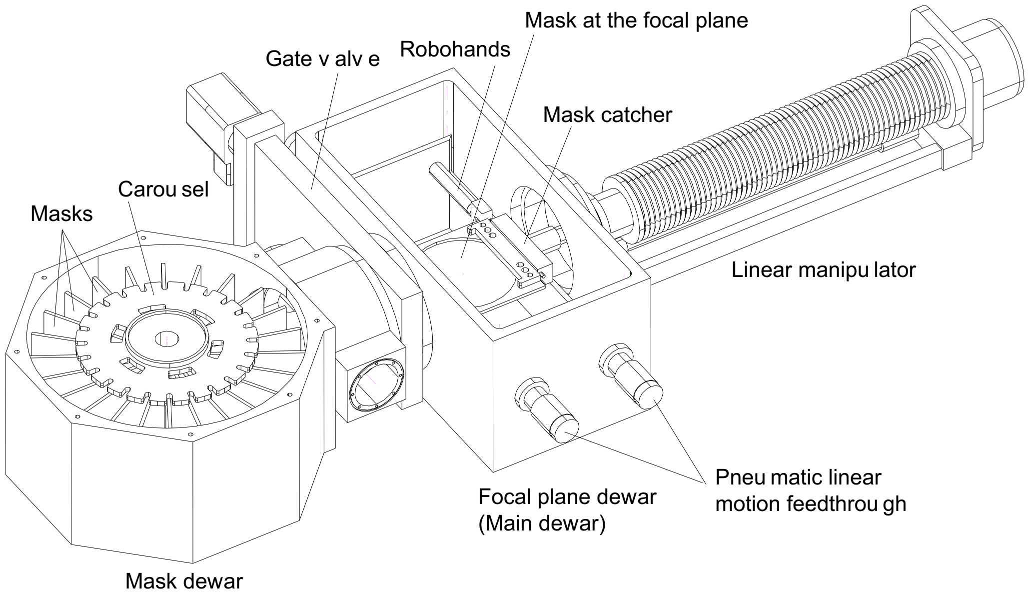

Figure 3. 3-D schematic view of the slit mask exchange system. The optical components are not shown in the figure.

designed to have a spectral resolution of $R{\sim}500$ in the first order. In addition, we are preparing an "$R1300$" grism which is designed to have a spectral resolution of $R{\sim}1300$ in the fourth, third, and second order for J-band, H-band, and K-band respectively. The specifications of the spectroscopic mode of MOIRCS is shown in Table 1.

Table 1. Multi-object spectroscopy characteristics.

Field of View	4×7 arcmin^2 (Imaging) 4×6 arcmin^2 (MOS)
Pixel Size	$0.''117$
Wavelength Coverage	0.85 - 2.5 μm (z, J, H, K-band)
Disperser	Grism
Resolution	500, 1300
Detectors	two of HAWAII-2 (2048 $\times$ 2048 pixels) arrays
Efficiency	$\sim$ 0.25 for $R500$ Grisms (J, H, and Ks-band)
Number of observable objects per mask	$\sim$ 20 - 50
Number of stored mask per night	17 + Long Slit Mask

2. MASK EXCHANGE SYSTEM

2.1. Mask Exchanger Mechanism

A 3-D schematic view of the mask exchanger is shown in Figure 3. The mask exchanger consists of a carousel, an arm with a mask catcher, and four robohands. The masks are held by the carousel. Eighteen masks are stored at once. The mask is gripped by the mask catcher and brought from the carousel to the focal plane of

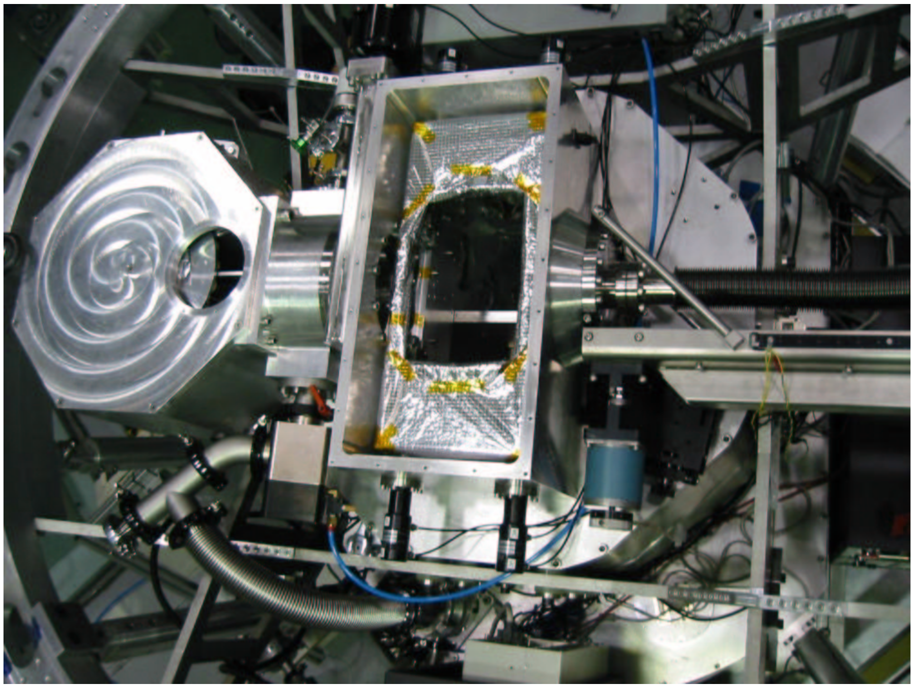

Figure 4. Top view of the slit mask exchange system. The optical components are not installed here.

the telescope by the arm. At the focal plane, the mask is gripped with the four robohands. The carousel sits on bearings and is driven by a stepping motor with a geneva gear, which is attached outside of the mask dewar. The geneva gear is shown in Figure 5.

In order to reduce thermal radiation from the mask surface itself, the masks are cooled to 150K or below. The masks stored in the mask dewar are attached to the carousel with magnets so they don't slide out during observations and are in good thermal contact for cooling. By rotating the carousel, one of the slots is selected by the arm to pick up the mask. The carousel rotates by $\pm$ 180°. The mask dewar has its own vacuum pump and cryocooler. The cryocooler cools the masks via the carousel and a heatpath. Since the heatpath is connected to the cold head, fixed to the mask dewar and to the carousel which rotates by $\pm$ 180° inside the dewar, the heatpath must be flexible. Oxygen-free high-conductivity (OFHC) copper straps are used for the heatpath, because OFHC material has high flexibility even in cryogenic environments. The number of layers was determined to maximize thermal conductivity without losing flexibility for the rotation of carousel.

Thermal transfer between the mask dewar and the carousel, however, should be minimized. The carousel is supported by the spoke-wheels made of stainless steel. Because the wheels are very thin and stainless steel has a small thermal conductivity, thermal transfer is reduced.

The arm is driven by a linear manipulator that moves the mask between the main dewar and the mask dewar. The linear manipulator achieves linear motion with high-precision for 500 mm of travel under an ultra-high vacuum. A combination of a stepping motor and sensors control the arm's motion. The mask is held by the mask catcher attached at the tip of the arm (Figure 6). A pneumatic feedthrough attached to the linear manipulator opens and closes the mask catcher.

The mask is held at the focal plane by 4 robohands during observations. The robohands are precision, 2-jaw parallel grippers with low friction and excellent part-position repeatability. In order to operate the robohands at cryogenic temperatures, we de-grease the gears and bearings. In order not to drop the masks on to the optics below the focal plane, the mask frame has small iron plates attached on its edges, which stick to the magnets in the robohands and mask catcher.

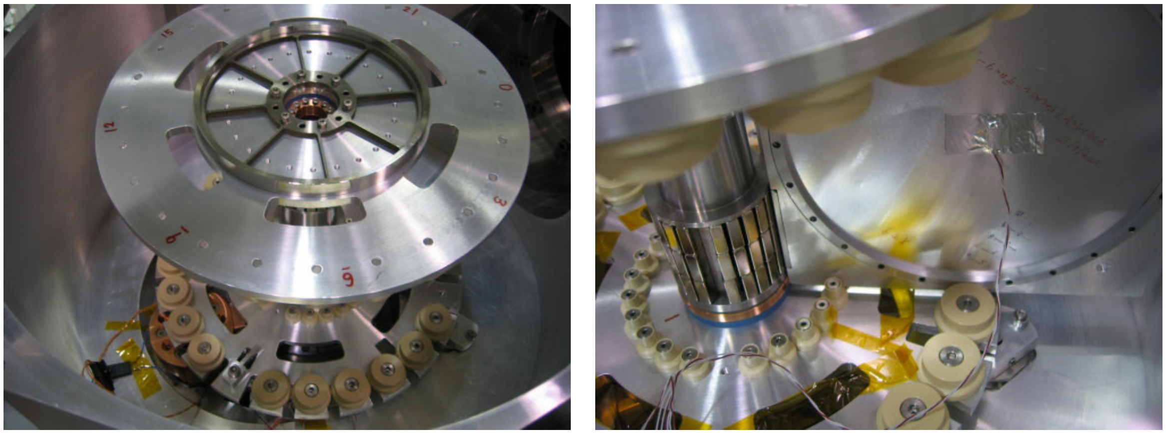

Figure 5. (Left) The carousel in the mask dewar. The geneva gear is shown at the lower right-hand corner. (Right) A mask is held by the carousel with magnets.

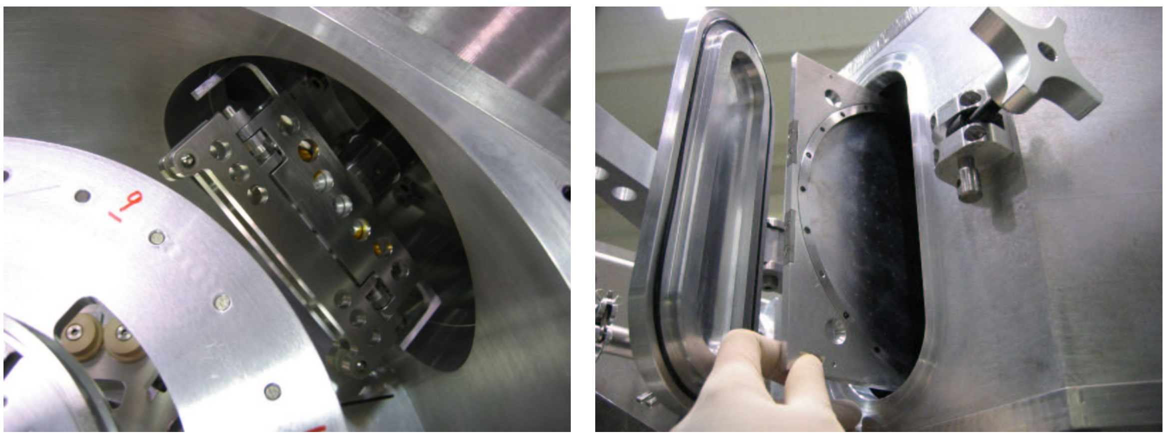

Figure 6. (Left) The mask catcher on the way to the mask dewar. It is rotated for clarity. (Right) Mask replacement from the side entrance of the mask dewar.

We use a gate valve between the two dewars to isolate the mask dewar from the main dewar during mask replacement. The gate valve has a 203mm diameter aperture and is operated electro-pneumatically. This valve allows us to break the vacuum in the mask dewar without affecting that in the main dewar.

2.2. Exchange Procedure

All the required movements during the mask exchange procedure are fulfilled by five fundamental sequences of actions: 1) The arm without a mask moves to the mask dewar from the initialized position (START). 2) The arm picks a mask from the carousel and fixes it in the focal plane (LOAD). 3) The arm returns the mask from the focal plane back to the mask dewar (STORE). 4) The arm moves the mask out of the focal plane for checking field (FCHECK). 5) The arm goes back to the initial position. All motions for mask exchange are the combination of several sequences of 1) to 5).

3. THE MASKS

3.1. The Selection of Mask Material

In order to keep the thermal radiation from the mask surface well below the background radiation from the sky, it is required to cool the masks to below 150K. For fast replacement of the mask set, the masks should be

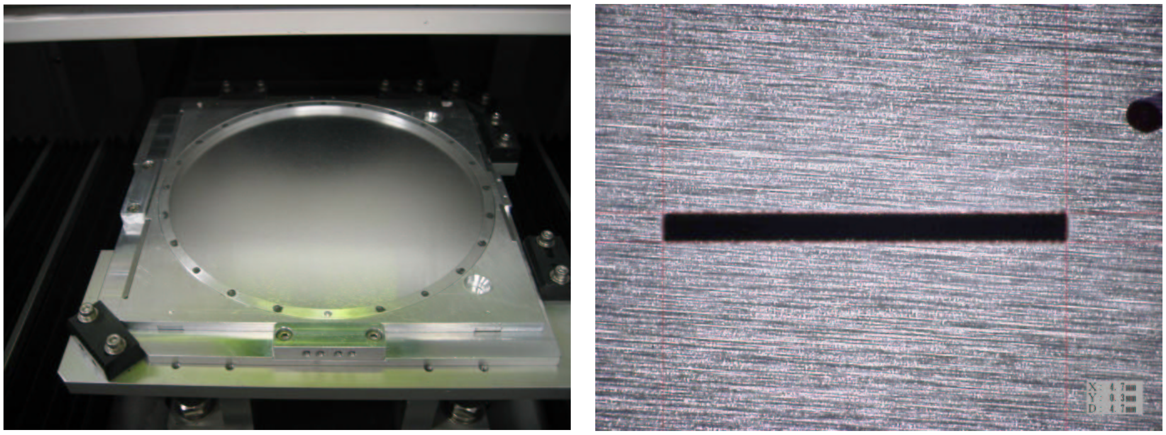

Figure 7. (Left) A mask with the maskframe on the laser cutter. (Right) The enlarged view of a slit cut (300 μm $\times$ 4.7 mm slits), which corresponds to $0.''6$ slit at the Subaru focus.

cooled as soon as possible. In addition, the mask material is required to have good thermal conductivity to help ensure for uniform temperature distribution. We chose to use hard-temper aluminum foil of 180mm diameter and 75μm (0.03 inches) thickness. Aluminum was chosen because it has both good thermal conductivity and good machinability.

3.2. Slit Cutting

Slits are cut with a diode-pumped YAG laser cutter, which is also used for the Faint Object Camera and Spectrograph (FOCAS)[5] slit mask cutting. The laser is operated at a wavelength of 1064 nm and has a power as high as 15W. The effects of thermal contraction during the cutting and optical distortion of the laser system is corrected by software. An enlarged view of a slit is shown in the right picture of Figure 7.

3.3. Thermal Contraction of the Masks

In order to make MOS masks for MOIRCS, it is fundamental to know the plate scale of the Cassegrain focus and the thermal contraction factor of the mask when it is cooled down to 150K. It is known that the distortion of the focal plane at the Cassegrain focus is negligible in a $\phi 6'$ central field (Kashikawa et al.[5]). In order to set the slits with $0.''1$ accuracy in the $6'$ field of view, the plate scale and the thermal contraction factor should be determined within 0.02% accuracy. The plate scale at the Cassegrain focus has been already accurately measured to be 2.06218 arcsec mm^{-1}. We now need to examine the thermal contraction factor of the mask. In addition, if the targets are selected from pre-imaging data taken with MOIRCS, the distortion of the image should be corrected before slit coordinates are determined.

Using pinhole masks and sky imaging data obtained with MOIRCS, we examined the thermal contraction factor. The important points are whether the thermal contraction is uniform or not and whether the thermal contraction factor is constant among different masks and different cooling runs. First, we prepared a distortion corrected and mosaicked sky image of several fields. We used the fields which contained many stars, like globular clusters placed pinholes at the positions of stars in the images. Only the plate scale at the Cassegrain focus was considered and no contraction factor was applied for the experiment. The pinhole masks were cooled in the mask dewar, installed in the focal plane, and imaged with MOIRCS without dispersing elements. The images were corrected for distortion- and mosaicked in the same way as for the sky images. Finally, the positions of the pinhole images were compared with the positions of stars in the sky images. The thermal contraction factor can then be directly measured by the comparison. We measured an average thermal contraction factor 1.0061 with a peak-to-peak difference of ± 0.0002, which is within the required specification (0.02%). The contraction is uniform and there is no significant residual after making the correction.

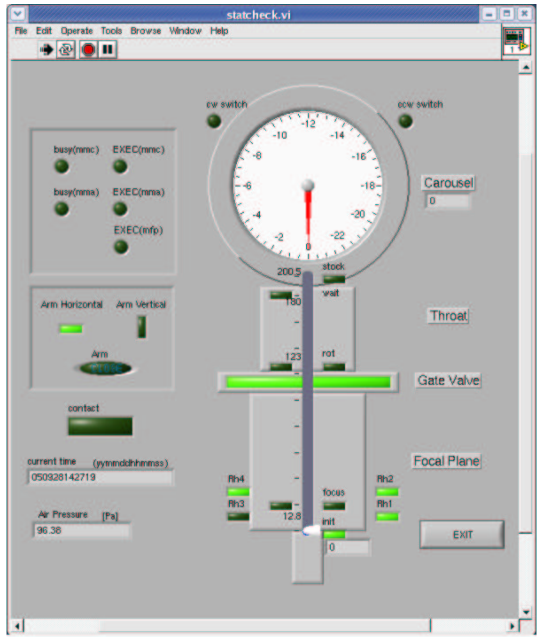

Figure 8. LabVIEW VI (virtual instrument) display for MOS control. Sensor buttons turn red if abnormal situations are detected.

The time variation of the thermal contraction factor after the mask installation was also measured. After about 100 hours of cooling, the contraction of the mask stopped. For most of the masks, at least 60 hours of cooling is required to reach a stable contraction factor of 1.0061±0.0002.

It is observed that the thermal contraction factor also changes at the focal plane. When the mask is at the focal plane, it is warmed by the thermal radiation through the MOIRCS window. The variation is large in the first 30min, but slows down later. The MOS acquisition procedure itself takes about 30min currently. Therefore the initial contraction is settled during the MOS acquisition sequence.

4. MOS SOFTWARE

4.1. Control System

Eight sensors of different types monitor the mask exchange process in the system: 4 micro switches, 4 photo micro sensors, 8 proximity sensors, one conductive switch, and a flow meter for pneumatic control. Each device is controlled either through an RS232C connection to a Lantronix terminal server or through relays connected to a Field Point Distributed I/O Control System manufactured by National Instruments, Inc.(NI). The terminal server and Distributed I/O are in turn controlled by TCP/IP through Ethernet. The control software for these housekeeping tasks was developed with LabVIEW, a GUI-based programming/development environment software by National Instruments, Inc (Figure 8). More detail about the control system is presented in Tokoku et al.(2003)[6] and Yoshikawa et al.(2006).[7]

4.2. Interlock

Exchanging masks with safety is important, especially under cryogenic conditions. For that purpose, macro commands which conduct the above sequences with proper confirmations of interlock conditions are crucial. Before conducting each step of the mask exchange procedures, interlock software checks all of the status from the sensors relevant to the step. No step is allowed to proceed until safe interlock conditions are met. The mask exchange can be done within 4 minutes, all automatically.

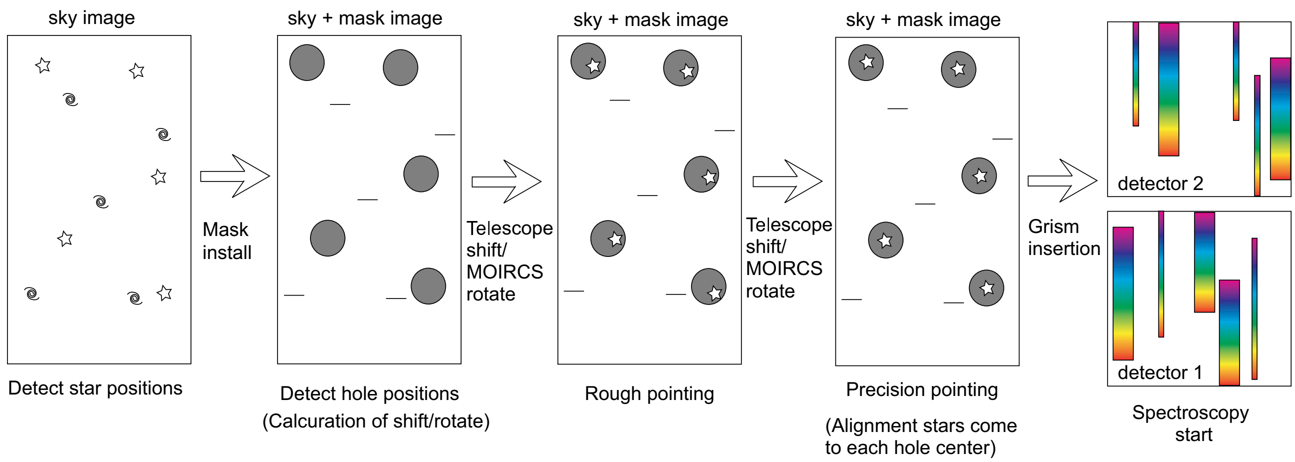

Figure 9. The sequence of the MOS pointing.

4.3. Mask Design Program

The mask design program for MOIRCS is under development. In order to design slit masks in the interim, we use the Mask Design Program (MDP) for Subaru's FOCAS instrument (Saito et al.[8]). Currently, images taken by MOIRCS, FOCAS, and Suprime-Cam are applicable as the pre-image.

5. MOS OBSERVATION

5.1. Pointing Sequence

The MOS pointing sequence for MOIRCS is the same in general as for the optical MOS instrument. The sequence is shown in Figure 9. At the start, we move the telescope to the target field, start guiding, and take the image of the field without a slit mask. Next, we install a mask and take a image of the mask. The position of the alignment stars and the guide holes on the masks are measured from the images. Based on the difference, the telescope is moved and/or the instrument rotator is rotated to the proper position. The alignment stars will be caught in the guiding holes. The star positions are measured again in the guiding holes. According to the offset of the stars in the guiding holes, the telescope or MOIRCS is again shifted and/or rotated, so that the stars come to the hole center. The iterations continue until the stars are centered in their holes within a certain accuracy.

Typical magnitudes of the alignment stars should be $K < 18$ mag. In fields at high galactic latitudes, the number of bright stars is usually limited and only faint alignment stars are available. Because the detection limit in near-infrared observations is generally shallower than in optical observations due to high background noise, we need to take two images with dithering to detect faint alignment stars. For example, we might take two images A and B slightly different positions, then subtract A from B. The subtracted image is used to find the faint stars for pointing. Currently, about 30 min is required to finish the pointing sequence.

We performed pointing tests in various types of regions: bright globular clusters, faint star clusters, and some deep survey regions. Thanks to the good pointing accuracy of the telescope, currently only a few iterations are required to reach a required accuracy $\sim 0.''1$ which is much smaller than the typical slit width for MOS observation, $0.''5 \sim 0.''8$.

5.2. Resolution

The spectral resolution of the grisms were measured with long-slit spectroscopic observations of night sky emission lines with $0.''3$ slits. The sky emission lines were selected from the OH-emission line atlas by Rousselot(2000).[9] The average spectral resolutions with $0.''3$ slits are 11.9Å and 13.8Å for the zJ500 and HK500 grisms, respectively.

The dispersion was also measured with the same data set. At first, the night sky emission lines in the data were identified with the OH-emission lines, then the wavelengths and the pixel coordinates were fitted with a

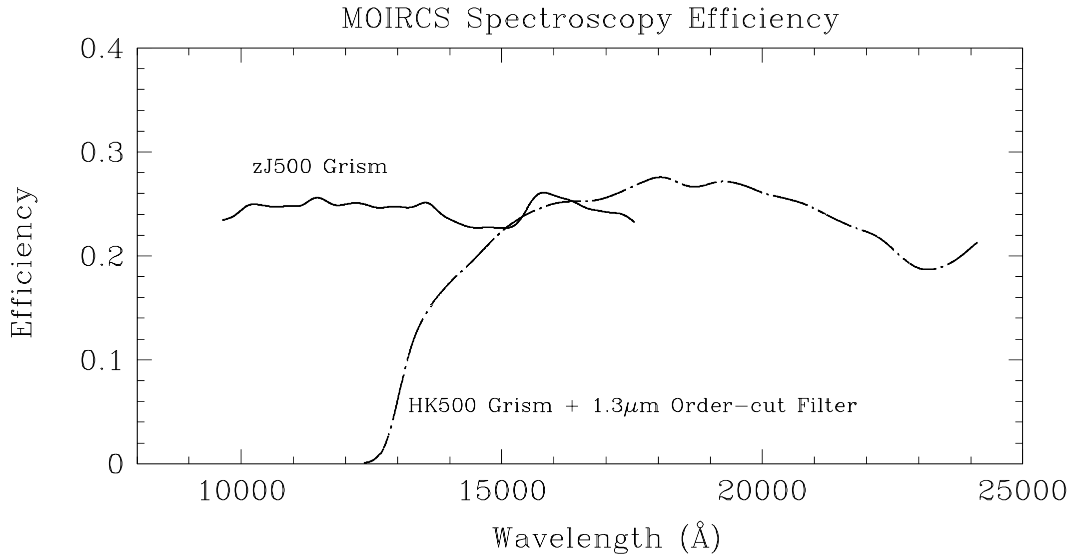

Figure 10. The efficiency of the MOIRCS spectrograph as measured by spectroscopic standard stars. The results includes filters, grating, detectors and the telescope.

polynomial function. The wavelengths were well fitted with 3rd order polynomial for both grisms with an rms residual of 0.5 pixel. The result indicates that the dispersions are 5.57 Å pixel^{-1} for the zJ500 grism and 7.72 Å pixels^{-1} for the HK500 grism in the first order.

5.3. Efficiency

In order to measure the spectroscopic efficiency of MOIRCS, we performed spectroscopic observations of an A0V spectroscopic standard star with known magnitude, M33570 (J=10.091mag, H=10.075mag, K=10.015 mag), on December 11, 2005. The zJ500 and HK500 grisms were used with $2.''0$ slit. Since the typical stellar image size during the observations was $0.''4$, almost all of the flux from the star was expected to fall in the slit. The data were taken at airmass 1.4. No filter was used for the zJ500 grisms, and a 1.3 μm order-cut filter was used for the HK500 grism.

The spectral images were flat-fielded with a normalized halogen lamp flat spectra. One dimensional spectral data were extracted from the flat-fielded data. The observed spectra were converted into photon flux (photons/s/Å) considering the gain of the detector, the integration time, and the spectral dispersion. The resulting efficiencies are shown in Figure 10. The efficiency include the telescope, optics, filters, grisms, and detectors.

5.4. Flat Fielding

For spectroscopic data, two types of flat light sources are available: one is a dome flat lamp illuminating the painted ceiling of the dome and the other is a slit illumination halogen lamp which is set just above the slit and illuminates the slit through a flat mirror. It should be noted that the illuminated area of the halogen lamp is limited, thus we need to sweep the lamp over the F.O.V. of the instrument.

5.5. Flexure of the Instrument

After a long integration, due to the flexure of the instrument, the relative position between the telescope and the mask, and between the mask and the detector can be changed. Target objects could be lost from the slit due to the former effect, while the position of the spectra on the detector can be shifted because of the latter effect.

Flexure tests of the instrument were done. A maximum shift of ± 2pix on the detector against a fixed light source was observed. The origin of this flexure is unknown. Such flexure can affect long integrations of spectroscopic observations.

5.6. Atmospheric Effects

Because the telescope does not have an atmospheric dispersion corrector (ADC) in the NIR wavelength, both differential atmospheric refraction inside the MOIRCS F.O.V. and atmospheric dispersion can affect target acquisition. The amount of the atmospheric refraction was calculated using the atmospheric refraction index provided in Roe(2002).[10] For atmospheric condition parameters, typical Mauna Kea values were assumed: a pressure of 603 millibar, temperature of 5°C, and a partial pressure of water vapor of 1.34 millibar. If acquisition is conducted in a band different from the spectroscopic observation, for example acquisition in the J-band and observation in the K-band, there can be a shift of targets due to atmospheric dispersion. The amount of image shift in the H and K-bands versus the J-band is negligible at zenith distances less than 45°, but needs to be considered when MOS acquisition is done at zenith distance (ZD) as large as 60° in the J-band and observed in the K-band.

Atmospheric dispersion also affects observations with long integration times. The telescope auto-guiding is done in the 730nm. Atmospheric dispersion between the observing wavelength and the guiding wavelength results in a shift of the target against the MOS mask. For example, if MOS acquisition is done at a ZD of 0°, the targets can be shifted $0\farcs19$ at a ZD of 30° in the K-band. If the observation continues down to a ZD of 60°, the amount of the shift reaches $0\farcs57$. The effect is differential, thus if the acquisition is done at a ZD of 45°, the shift will be $0\farcs57$ - $0\farcs33$ = $0\farcs24$ at a ZD=60° in the K-band.

Finally, the atmospheric effects also affect mask design. For example, if a pre-image is obtained at ZD=60° and the MOS observation for the field is conducted at ZD=0°, there will be $0\farcs28$ - $0\farcs07$ = $0\farcs21$ difference in the distance between the stars at the both edges of the F.O.V. The amount of the differential atmospheric refraction is almost same in all of the three bands.

ACKNOWLEDGMENTS

We would like to thank the members of the Subaru Telescope: the daycrews, the night operators, and the laboratory technicians for their great help. We would also like to thank Kerry Martin for his machining work. This research was supported by grant-in-aid from scientific research of the Ministry of Education, Culture, Sports, Science and Technology (09440088, 11554005, and 14300059).

REFERENCES

1. T. Ichikawa, D. Matsumoto, K. Yanagisawa, Y. Katsuno, R. Suzuki, C. Tokoku, K. Asai, and T. Nishimura, "Tohoku University Focal Plane Array Controller (TUFPAC)," in *SPIE: Instrument Design and Performance for Optical/Infrared Ground-based Telescopes*, M. Iye and A. F. Moorwood, eds., *Proc. SPIE* **4841**, p. 376, 2003.
2. Y. Katsuno, T. Ichikawa, K. Asai, R. Suzuki, C. Tokoku, and T. Nishimura, "Performance tests of hawaii-2 FPAs for MOIRCS," in *SPIE: Instrument Design and Performance for Optical/Infrared Ground-based Telescopes*, M. Iye and A. F. Moorwood, eds., *Proc. SPIE* **4841**, p. 271, 2003.
3. R. Suzuki, C. Tokoku, T. Ichikawa, and T. Nishimura, "Optical design of MOIRCS," in *SPIE: Instrument Design and Performance for Optical/Infrared Ground-based Telescopes*, M. Iye and A. F. Moorwood, eds., *Proc. SPIE* **4841**, p. 307, 2003.
4. T. Ichikawa, R. Suzuki, C. Tokoku, Y. Katsuno, M. Konishi, T. Yoshikawa, T. Yamada, I. Tanaka, K. Omata, and T. Nishimura, "MOIRCS: Multi-Object Infrared Camera and Spectrograph," in *SPIE: Ground-based and Airbone Instrumentation for Astronomy*, I. S. McLean and M. Iye, eds., *Proc. SPIE* **6269**, 2006.
5. N. Kashikawa, K. Aoki, R. Asai, N. Ebizuka, M. Inata, M. Iye, K. S. Kawabata, G. Kosugi, Y. Ohyama, K. Okita, T. Ozawa, Y. Saito, T. Sasaki, K. Sekiguchi, Y. Shimizu, H. Taguchi, T. Takata, Y. Yadoumaru, and M. Yoshida, "Focas: The Faint Object Camera and Spectrograph for the Subaru Telescope," *PASJ* **54**, p. 819, 2002.
6. C. Tokoku, R. Suzuki, T. Ichikawa, K. Asai, Y. Katsuno, K. Omata, T. Yamada, A. Sasaki, and T. Nishimura, "MOIRCS: Multi-Object Infrared Camera and Spectrograph for the Subaru Telscope," in *SPIE: Instrument Design and Performance for Optical/Infrared Ground-based Telescopes*, M. Iye and A. F. Moorwood, eds., *Proc. SPIE* **4841**, p. 1625, 2003.

7. T. Yoshikawa, K. Omata, M. Konishi, T. Ichikawa, R. Suzuki, C. Tokoku, Y. Katsuno, and T. Nishimura, "The application of SQL database server to the control system of MOIRCS," in *SPIE: Advanced Software and Control for Astronomy*, M. J. Cullum and G. Z. Angeli, eds., *Proc. SPIE* **6274**, 2006.
8. Y. Saito, Y. Ohyama., N. Kashikawa, M. Yoshida, T.Sasaki, G. Kosugi, T. Takata, Y. Shimizu, M. Inata, K. Okita, K. Aoki, K. Sekiguchi, K. S. Kawabata, R. Asai, H. Taguchi, N. Ebizuka, Y. Yadoumaru, T. Ozawa, and M. Iye, "Multi-object spectroscopy of FOCAS: software and its performance," in *SPIE: Instrument Design and Performance for Optical/Infrared Ground-based Telescopes*, M. Iye and A. F. Moorwood, eds., *Proc. SPIE* **4841**, p. 1180, 2003.
9. P. Rousselot, C. Lidman, J. G. Cuby, G. Moreels, and G. Monnet., "Night-sky spectral atlas of OH emission lines in the near-infrared," *A&A* **354**, p. 1134, 2000.
10. H. G. Roe, "Implications of atmospheric differential refraction for adaptive optics observations," *PASP* **114**, p. 450, 2002.